Resonant fiber scanner with optical feedback

M. H. H. Mokhtar* **and R. R. A. Syms**

Electrical and Electronics Engineering Dept., Imperial College London, Exhibition Road, London SW7 2AZ, UK
**m.mokhtar11@imperial.ac.uk*

Abstract: The addition of an apertured mirror before the imaging lens is proposed as a method of providing feedback in a single-axis resonant fiber scanner. Reflection at the scan extremities generates timing signals interlaced with back-scattered data, and a phase locked loop and a proportional controller then adjust the drive frequency and amplitude. The capture range and stability of the system are examined. Verification is obtained using a confocal scanner based on mechanically biaxial fiber.

OCIS codes: (060.2350) Fiber optics imaging; (120.5800) Scanners.

References and links

1. K. E. Petersen, "Silicon torsional scanning mirror," IBM J. Res. Develop. **24**(5), 631–637 (1980).
2. H. Toshiyoshi, G. D. J. Su, J. LaCosse, and M. C. Wu, "A surface micromachined optical scanner array using photoresist lenses fabricated by a thermal reflow process," J. Lightwave Technol. **21**(7), 1700–1708 (2003).
3. G. Zhou and F. S. Chau, "Micromachined vibratory diffraction grating scanner for multiwavelength collinear laser scanning," J. Microelectromech. Syst. **15**(6), 1777–1788 (2006).
4. H. Urey, "Torsional MEMS scanner design for high-resolution display systems," Proc. SPIE **4773**, 27–37 (2002).
5. M.-H. Kiang, O. Solgaard, R. S. Muller, and K. Y. Lau, "Micromachined polysilicon microscanners for barcode readers," IEEE Photon. Technol. Lett. **8**(12), 1707–1709 (1996).
6. H. Miyajima, N. Asaoka, T. Isokawa, M. Ogata, Y. Aoki, M. Imai, O. Fujimori, M. Katashiro, and K. Matsumoto, "A MEMS electromagnetic optical scanner for a commercial confocal laser scanning microscope," J. Microelectromech. Syst. **12**(3), 243–251 (2003).
7. W. Piyawattanametha, R. P. J. Barretto, T. H. Ko, B. A. Flusberg, E. D. Cocker, H. Ra, D. Lee, O. Solgaard, and M. J. Schnitzer, "Fast-scanning two-photon fluorescence imaging based on a microelectromechanical systems two- dimensional scanning mirror," Opt. Lett. **31**(13), 2018–2020 (2006).
8. L. Giniunas, R. Juskaitis, and S. V. Shatalin, "Scanning fiber-optic microscope," Electron. Lett. **27**(9), 724–726 (1991).
9. D. A. Roberts, R. R. A. Syms, A. S. Holmes, and E. M. Yeatman, "Dual numerical aperture confocal operation of a moving fiber bar-code reader," Electron. Lett. **35**(19), 1656–1658 (1999).
10. F. Helmchen, M. S. Fee, D. W. Tank, and W. Denk, "A miniature head-mounted two-photon microscope. high-resolution brain imaging in freely moving animals," Neuron **31**(6), 903–912 (2001).
11. B. A. Flusberg, J. C. Jung, E. D. Cocker, E. P. Anderson, and M. J. Schnitzer, "In vivo brain imaging using a portable 3.9 gram two-photon fluorescence microendoscope," Opt. Lett. **30**(17), 2272–2274 (2005).
12. J. Sawinski, D. J. Wallace, D. S. Greenberg, S. Grossmann, W. Denk, and J. N. D. Kerr, "Visually evoked activity in cortical cells imaged in freely moving animals," Proc. Natl. Acad. Sci. U.S.A. **106**(46), 19557–19562 (2009).
13. E. C. Haight and W. W. King, "Stability of nonlinear oscillations of an elastic rod," J. Acoust. Soc. Am. **52**(3B), 899–911 (1972).
14. Q. Y. J. Smithwick, P. G. Reinhall, J. Vagners, and E. J. Seibel, "A nonlinear state-space model of a resonating single-fiber scanner for tracking control: theory and experiment," J. Dyn. Syst. Meas. Control **126**(1), 88–101 (2004).
15. D. A. Roberts and R. R. A. Syms, "1D and 2D laser line scan generation using a fiber optic resonant scanner," SPIE Proc. **4075**, 62–73 (2000).
16. R. D. Birch, D. N. Payne, and M. P. Varnham, "Fabrication of polarization-maintaining fibers using gas-phase etching," Electron. Lett. **18**(24), 1036–1038 (1982).

1. Introduction

Since the development of micro-electro-mechanical systems technology, there has been interest in scanning systems based on moving optical components. The most common are based on mirrors [1], lenses [2] and diffraction gratings [3], and their applications include displays [4], bar-code scanners [5] and microscopes [6], especially for biomedical imaging

#216427 - $15.00 USD Received 7 Jul 2014; revised 3 Sep 2014; accepted 7 Sep 2014; published 13 Oct 2014

[7]. It is simple to provide the feedback needed for closed-loop control, using capacitive, piezoelectric or optical sensing; however, additional optics is required for data collection.

Alternative systems are based on single-mode fibers that are mechanically scanned before an imaging lens to create a 1-D scan or a 2-D pattern such as a Lissajous Fig [8–12]. Confocal detection may be implemented easily, by coupling the scattering from the target back into the fiber. The signal may be increased by illuminating the target using a beam from core and collecting the scattering in the cladding [9]. Unfortunately, performance is often poor. Cross-coupled non-linear oscillations may be excited in a fiber with equal principal second moments, leading to elliptical scans when only a linear scan is desired [13], and uncertainty in the origin of the data. Although controllers have been developed, the focus has been on countering non-linearity, using feedback from the scan pattern itself [14].

Undesirable dynamical effects can be minimised using fibers with non-degenerate resonances. Suitable results can be achieved using standard fiber with an etched cladding [15]; alternatives include polarization-preserving fibers [16]. However, even then, there may be unknown phase shifts between the drive and response away from resonance. Consequently, there is a need for simple position sensors. The aim of this paper is to investigate the use of intermittent reflection to provide feedback for phase and amplitude tuning. All that is required is the addition of an apertured reflector before the imaging lens, making the approach simple to implement. The system is introduced in Section 2, and a model of the controller in Section 3. Experimental results are presented in Section 4 and conclusions are drawn in Section 5.

2. Scanner design

Figure 1(a) shows a dual numerical aperture (NA) confocal resonant fiber scanner [9]. Light from a laser diode is butt-coupled into a fiber, using a mode stripper to eliminate cladding modes. The free end of the fiber is placed close to a gradient index (GRIN) lens, which forms a magnified image of the guided mode. Near its free end, the fiber is mounted on a piezoelectric transducer, forming a short cantilever. The transducer is driven with a sinusoidal voltage v(t) from a control PC so that the cantilever is resonant and a scan line is formed. Light is scattered from a target in the image plane, and diffuse light passes back through the lens to form an image at the fiber tip. The return is coupled back into the fiber, with low and high NA components in the core and cladding respectively. Cladding modes are coupled into a photodiode between the fiber and the transducer. Assuming the fiber mode has a numerical aperture N_F, and that collection is limited by the numerical aperture N_L of the lens, the power gain over a single-NA system with a beam-splitter is $G = 4\ (NA_L^2 - NA_F^2) / NA_F^2$. If $N_L >> N_F$, G is large, leading to an increase in the possible target range, by a factor of $\approx G^{1/2}$.

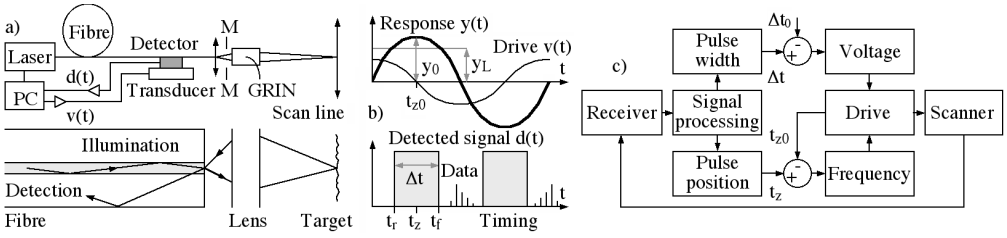

Fig. 1. Resonant fiber scanner, a) system b) ideal variations of drive, response and signal c) controller.

To maximise the response, the drive frequency f should match the lowest order resonant frequency f_{01} of the cantilever. At resonance, the response y(t) should then vary sinusoidally, but lag in phase by 90° as shown in Fig. 1(b). However, if the scan amplitude y_0 is greater than the radius y_L of the lens, light will be reflected into the cladding by a mirror M at the scan extremities. The detected signal d(t) will consist of periodic repetitions of the target return, interlaced with timing pulses. However, if the drive is off-resonance there will be a phase shift between the ideal and actual response, and an error in the scan amplitude, leading to uncertainty in the origin and the size scale of the data. These aspects require active control.

#216427 - $15.00 USD Received 7 Jul 2014; revised 3 Sep 2014; accepted 7 Sep 2014; published 13 Oct 2014

A controller to lock the drive frequency and voltage can be developed as shown in Fig. 1(c). Two loops are shown; these operate sequentially. The frequency loop operates first. Measurement of the rise and fall-times t_r and t_f from a single pulse allows the pulse position to be estimated as $t_Z = (t_f + t_r)/2$, and the deviation of t_Z from the zero-crossing point t_{ZS} of the drive is used to iterate the frequency in a discrete-time control loop. The voltage loop operates second. Measurement of t_f and t_r allows the pulse width to be estimated as $\Delta t = (t_f - t_r)$, and the deviation of Δt from a set value Δt_S is then used to iterate the voltage. In each case, the loops are assumed to operate slowly enough that steady-state analysis may be used to estimate the system response; however it is likely that much faster operation can be achieved.

3. Controller design

A vibrating cantilever is of course a distributed resonant system, with a set of distinct resonant modes. Standard theory gives the angular resonant frequency ω_{0n} of the n^{th} mode as:

$$\omega_{0n} = \left(\alpha_n / L^2\right)\sqrt{\left(EI/\rho A\right)} \tag{1}$$

Here L, A and I are the length, cross-sectional area and second moment of area of the fiber, and ρ and E are the density and Young's modulus. α_n is a numerical constant from the dynamic beam-bending equation. For a cylindrical cross-section, $I = \pi r^4/4$, and $\alpha_1 = 3.516$ and $\alpha_2 = 22.034$ for the 1st and 2nd modes, giving a ratio 6.27 between ω_{02} and ω_{01}. For (say) a length L = 25 mm of 125 μm diameter silica fiber ($\rho \approx 2200$ kg/m^3; $E \approx 73.1 \times 10^9$ N/m^2), we obtain $f_{01} = \omega_{01}/2\pi \approx 160$ Hz and $f_{02} \approx 1$ kHz. The primary resonance is low enough for computation during iteration. To good approximation, the response near f_{01} can be modelled as that of a mass-spring-damper system. The complex amplitude y_0 at angular frequency ω is:

$$y_0 = v_0 C \Big/ \left\{\left(\omega_{01}{}^2 - \omega^2\right) + 2j\zeta\omega\omega_{01}\right\} \tag{2}$$

Here v_0 is the drive voltage of the excitation system, C is a scaling coefficient, and ζ is the damping coefficient. Maximum amplitude $y_{Max} = v_0 C/2\zeta\omega_{01}{}^2$ is obtained at resonance. Figure 2(a) shows the variation of $|y_0/y_{Max}|$ with f/f_{01} for the typical damping factor ζ = 0.005, while Fig. 2(b) shows the corresponding variation of the phase $\phi = \arg(y_0)$. The response is clearly high only when the angular frequency deviation $\Delta\omega = \omega_{01} - \omega$ is small. In this range:

$$\phi \approx -\tan^{-1}\left(\zeta\omega_{01}/\Delta\omega\right) \tag{3}$$

Exactly at resonance, the phase passes through the set point $\phi_S = -\pi/2$. Near this point, φ varies quasi-linearly with Δω, following the approximate relation:

$$\phi - \phi_s \approx \Delta\omega \Big/ \left(\zeta\omega_{01}\right) \tag{4}$$

This relationship is plotted as a dashed line; clearly, it is a reasonable approximation over a small frequency range but deviates considerably outside this range.

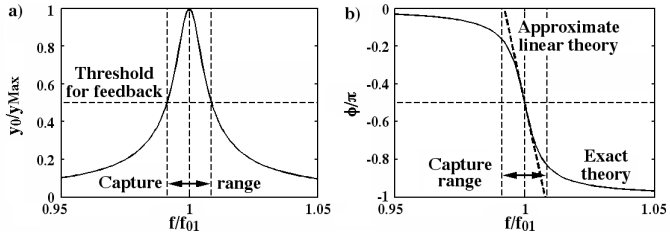

Fig. 2. Theoretical open-loop frequency dependence of a) amplitude and b) phase, for ζ = 0.005.

#216427 - $15.00 USD Received 7 Jul 2014; revised 3 Sep 2014; accepted 7 Sep 2014; published 13 Oct 2014

To analyse the voltage loop, we consider the time response after the frequency loop has converged to resonance. For a more general voltage amplitude v, the response is $y(t) = (v/v_0)\, y_{max} \sin(\omega t)$. Shifting the time origin to a response peak, we obtain $y(\tau) = (v/v_0)\, y_{max} \cos(\omega\tau)$ where $\omega\tau = \omega t - \pi/2$. The amplitude therefore reaches y_L (so a feedback pulse edge is generated) when $(v/v_0)\, y_{max} \cos(\omega\tau) = y_L$. This observation allows the voltage to be related to the phase difference $\Delta\phi = \omega\tau$ between the zero crossing of the drive and the pulse edge as:

$$v = a / \cos(\Delta\phi) \tag{5}$$

Here $a = v_0(y_L/y_{Max})$. Equations (4) and (5) are key to the operation of the two loops. A feedback signal is only obtained if $|y_0| > y_L$, so that the normalised peak amplitude $|y_0/y_{Max}|$ must lie above a defined level (taken arbitrarily as 0.5 in Fig. 2(a)). This requires

$$4\zeta^2\omega_{01}{}^4 \Big/ \left\{ \left(\omega_{01}{}^2 - \omega^2\right)^2 + 4\zeta^2\omega^2\omega_{01}{}^2 \right\} > \left(y_L / y_{max}\right)^2 \tag{6}$$

For low damping, a useful response will only be obtained close to resonance. Assuming that $\omega = \omega_{01} - \Delta\omega$ once again, we can extract the capture range $\Delta\omega_C$ as:

$$\Delta\omega_C / \omega_{01} = \zeta \sqrt{\left\{ \left(y_{max}/y_L\right)^2 - 1 \right\}} \tag{7}$$

The capture range is clearly zero (so the algorithm fails) for $y_{max}/y_L \le 1$, then rises rapidly, and finally tends to the straight-line asymptote $\Delta f_C/f_{01} = \zeta y_{max}/y_L$. For a system with $y_{max}/y_L = 2$ (say), $\Delta f_C/f_{01} = 0.0173$. This value is very small, indicating that the system must be close to resonance prior to operation of the frequency control loop.

We now consider the frequency iteration algorithm, which has the form:

$$\omega_{n+1} = \omega_n - k_\omega \left(\phi_n - \phi_S\right) \tag{8}$$

Here k_ω is a feedback gain for angular frequency. Subtracting ω_{01} from both sides and substituting for $\phi_n - \phi_S$ using (3) we then get:

$$\Delta\omega_{n+1} = \Delta\omega_n \left(1 - \alpha\right) \tag{9}$$

Here $\alpha = k_\omega/\zeta\omega_0$. Hence, iteration from general starting condition $\Delta\omega_0$ must follow $\Delta\omega_n = \Delta\omega_0(1 - \alpha)^n$. This evolution depends on the value of α. If it is small, $\Delta\omega_n \approx \Delta\omega_0 \exp(-n\alpha)$ and the error declines exponentially. If α is greater than 1, $\Delta\omega_n$ will change sign at each iteration, but still converge to zero if $\alpha < 2$. Conversely, if $\alpha > 2$, the oscillations will grow. A similar calculation can be performed, assuming that $\Delta\omega_0$ is so large that the approximation (4) is no longer valid. To illustrate the difference, Fig. 3(a) shows the theoretical variation of $\Delta f_n/\Delta f_0$ with n for an initial frequency error $\Delta f_0/\Delta f_C = 0.0625$, a damping factor $\zeta = 0.005$, a scan amplitude $y_{max}/y_L = 2$ and α-values of 0.5, 1.0, 1.5, 2.0 and 2.5. Here, the initial error is a small fraction of the capture range and the approximation is accurate. For low α, convergence is approximately exponential, but for high α diverging oscillations occur. In Fig. 3(b), $\Delta f_0/\Delta f_C$ is raised to 0.5, and (4) is breaking down. Again, for low α, convergence is approximately exponential, but for high α, limit cycle oscillations now occur.

Finally, we consider the voltage control loop. Assuming that the frequency loop has forced the system into resonance, the voltage iteration algorithm has the form:

$$v_{n+1} = v_n - k_v \left\{ 1/\cos\left(\Delta\phi_n\right) - 1/\cos\left(\Delta\phi_S\right) \right\} \tag{10}$$

Substituting using (5) then gives:

$$v_{n+1} = v_n - \left(k_v / a\right)\left(v_n - v_S\right) \tag{11}$$

#216427 - $15.00 USD Received 7 Jul 2014; revised 3 Sep 2014; accepted 7 Sep 2014; published 13 Oct 2014

Here $v_S = a/\cos(\Delta\phi_S)$ is a set-point voltage that may easily be calculated. Defining the voltage error Δv_n as $\Delta v_n = v_n - v_S$, we obtain:

$$\Delta v_{n+1} = \Delta v_n (1-\beta) \tag{12}$$

Here $\beta = k_v/a$. Iteration from a starting condition Δv_0 must then follow $\Delta v_n = \Delta v_0(1 - \beta)^n$, so the voltage error will decline exponentially provided β is small, oscillations will occur if $\beta > 1$, and instability if $\beta > 2$. However, smaller values of β must generally be used, to avoid loss of feedback at low scan amplitude. Figure 3(c) shows the theoretical variation of $\Delta v_n/\Delta v_0$ with n, for β-values of 0.5, 1.0 and 1.5. For low β, convergence is exponential; for high β, oscillations occur. The lower plots show comparative experimental results; these will be discussed later.

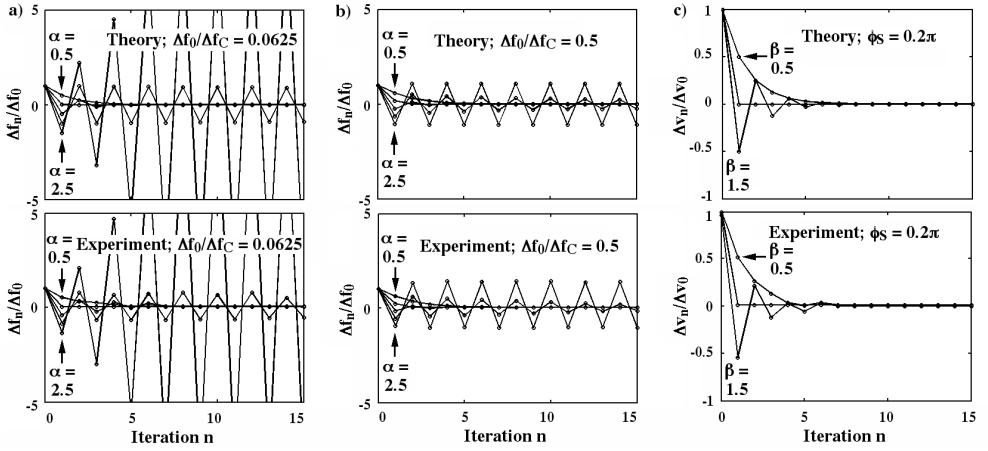

Fig. 3. a) and b) Convergence of frequency error $\Delta f_n/\Delta f_0$, for initial errors of $\Delta f_0/\Delta f_C = 0.0625$ and 0.5, assuming $\zeta = 0.005$, $y_{max}/y_L = 2$; c) Convergence of voltage error, assuming $\phi_S = 0.2\pi$.

4. Experimental verification

Experiments were carried out using the breadboard scanner in Figs. 4(a) and 4(b). The source was a 635 nm wavelength laser diode coupled to a fiber with a cantilever length of 25 mm. To avoid degenerate resonances, this fiber was bow-tie type [15], with the cross-section in the inset to Fig. 4(b). The transducer was a piezoelectric diaphragm. The detector was a surface-mount PIN photodiode with a transimpedance amplifier. The lens was a 1.8 mm diameter, 0.23-pitch AR-coated GRIN lens. The aperture mirror was a 1.5 mm wide slot in 75 μm thick photoetched steel. The fiber and lens were mounted on an x-y-z stage, and the mirror was attached to the lens mount. The drive signal was generated using a sound card and sampled at 44.1 kS/sec. The controller was implemented in MATLAB; data was acquired over a number of cycles, the pulse edges extracted, and the controller used to apply new scan parameters.

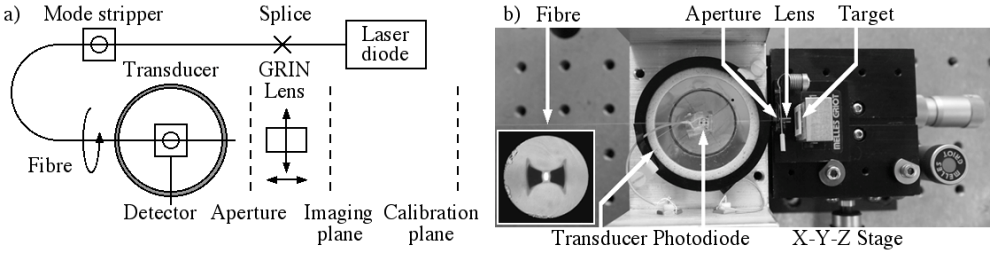

Fig. 4. Breadboard scanner: a) schematic and b) experimental rig.

#216427 - $15.00 USD Received 7 Jul 2014; revised 3 Sep 2014; accepted 7 Sep 2014; published 13 Oct 2014

The mechanical response of the fiber was characterised by observing scan patterns in a far-field plane. In general, the pattern was elliptical and oblique. However, linear scans could be obtained by rotating the fiber to angles when the vertical direction coincided with a principal axis. The fiber was then rotated through 45°, so that the two modes could be excited simultaneously. The length of the resulting elliptical scan was then measured in directions at ± 45° to the vertical, allowing the frequency responses of both modes to be measured. Figure 5(a) shows the result. The resonant frequencies differ by ≈2.5%, implying a difference in principal second moment of ≈5%. The responses overlap, and there is evidence of non-linear coupling. Despite this, linear scans were obtained when the fiber was aligned correctly.

The fiber was then rotated to force excitation of the high-frequency mode and glued in place. Figure 5(b) shows the frequency response of the linear scan thus obtained, on an expanded scale. The 1st and 2nd resonances can be seen, differing in frequency by the theoretical ratio 6.27. Figure 5(c) shows more detailed response characteristics near the primary resonance (≈162.5 Hz), matched to the theory of Eq. (2). The voltage response and damping factor $\zeta = 0.005$ were then used to estimate the value of α.

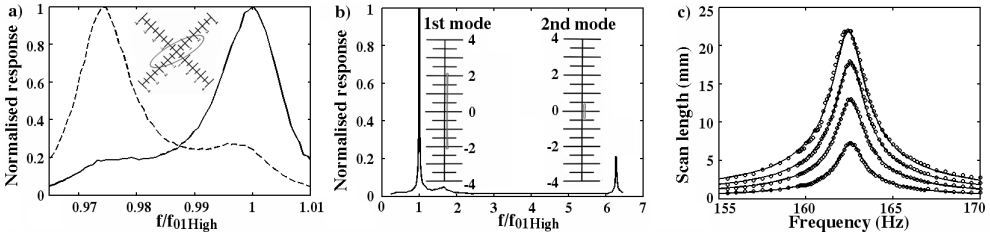

Fig. 5. Responses of bow-tie fibers with principle axes a) at ± 45° and b) and c) at 0° to vertical.

Closed loop responses were obtained from a bar-code target ≈1 mm from the lens. Figure 6(a) shows time variations in the drive and signal at resonance, assuming that $y_{max}/y_L = 2$. The feedback pulse heights are unequal, due to a tilt in mirror M. Similar effects – unequal pulse widths – are caused by transverse misalignment. Figures 6(b) and 6(c) show drive and return signals at the start and end of the control loop, with the system properly set up, but with an initial frequency error of $\Delta f_0/\Delta f_C = 0.5$ and an excessive scan amplitude. Initially, the pulse centres do not coincide with the zero-crossings of the drive. In Fig. 6(c), the frequency error has been eliminated and the pulse width reduced. Comparison of the effect of the parameters α and β with theory is shown in Fig. 3. In each case, controller functions as expected.

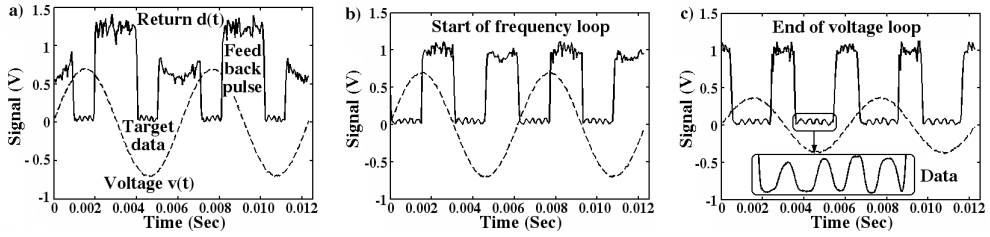

Fig. 6. Time variation of drive and signal, for a) misaligned system, b) start and c) end of control loop.

5. Conclusion

Intermittent feedback in a single-axis resonant fiber scanner has been demonstrated, based on an apertured mirror in front of the imaging lens. Reflection at the scan extremities generates timing signals interlaced with back-scattered data, and a phase locked loop and a proportional controller are used to set the frequency and amplitude. Convergence and stability have been examined theoretically, and verification obtained using a piezoelectrically actuated confocal scanner. The approach is simple to implement, but requires the fiber to over-scan the lens.

#216427 - $15.00 USD Received 7 Jul 2014; revised 3 Sep 2014; accepted 7 Sep 2014; published 13 Oct 2014